Nanoscale

Accepted Manuscript

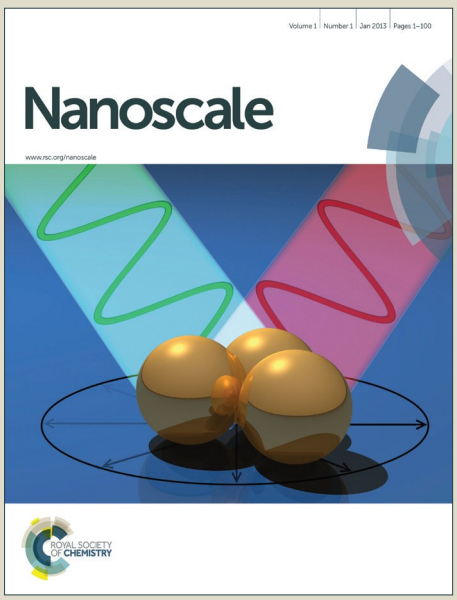

ROYAL SOCIETY OF CHEMISTRY

www.rsc.org/nanoscale

Journal Name

ARTICLE

Magnetic Response of hybrid ferromagnetic and antiferromagnetic core-shell nanostructures

Received 00th January 20xx,
Accepted 00th January 20xx

DOI: 10.1039/x0xx00000x

www.rsc.org/

U. Khan,[a,*] Wenjing Li,[a] N. Adeela,[b] M. Irfan,[a] K. Javed,[a] S. Riaz,[a] and X. F. Han[a,*]

The synthesis of $FeTiO_3$-Ni($Ni_{80}Fe_{20}$) core-shell nanostructures by two step method (sol-gel and DC electrodeposition) has been demonstrated. XRD analysis proved the rhombohedral crystal structure of $FeTiO_3$(FTO) with space group $R\bar{3}$. Transmission electron microscopy clearly depicts better morphology of nanostructures with shell thickness of ~25nm. Room temperature magnetic measurements showed significant enhancement of magnetic anisotropy for permalloy ($Ni_{80}Fe_{20}$)-FTO over Ni-FTO core-shell nanostructures. Low temperature magnetic measurements of permalloy-$FeTiO_3$ core-shell structure proposed strong exchange bias mechanism with magnetic coercivity below antiferromagnetic Neel temperature (T_N=59K). The exchange bias is attributed to the alignment of magnetic moments in antiferromagnetic material at low temperature. Our scheme opens a path towards optimum automotive systems and wireless communications where broader bandwidths and smaller sizes are required.

Introduction

Magnetic nanostructures are of prime interest due to their fascinating and attractive properties as compared with their bulk counterparts. The size dependency of various nanostructures offers completely different and unexpected behaviour which highly allows their presence for innovative scientific research and potential industrial applications.[1-2] One-dimensional (1D) nanostructures are also stimulating incredible role as both functional units and interconnection for the fabrication of magnetic recording media,[3] magnetic memories,[4] sensors,[5] and microwave devices[6] in nanotechnology industry. Among several magnetic properties exchange bias (EB) has important technological applications. It has been reported that nanostructures can exhibit EB in ferromagnetic (FM), anti-ferromagnetic (AFM) and ferrimagnetic systems depending on variable sizes.[7] EB can also occur in zero-dimensional (core-shell nanoparticles),[8] one-dimensional (core-shell nanowires/nanotubes),[9-10] and two-dimensional (FM/AFM thin films)[11] system. Non-volatility, high speed, and reduced power consumption are the essential elements for the development in spintronic devices.[12] Exchange biased devices plays crucial role for this improvement in spin valves and magnetic tunnel junctions.[13] Temperature dependent EB has been studied extensively. Meanwhile, temperature dependent magnetic coercivity H_c can perform several magnetic mechanisms depending on induced magnetic anisotropy of AFM material.[14] $FeTiO_3$ is an antiferromagnetic material (Neel temperature of ~59 K and Curie temperature of 1000 K which can produce large anisotropy with band gap of 2.58-2.9 eV.[15-19] The materials with wide band gap are suitable for electronic devices, spintronic applications, high temperature integrated circuits etc.[16] Hence, $FeTiO_3$ is a potential candidate for such applications. It has been reported that $FeTiO_3$ is AFM material with rhombohedral crystal structure. The study about crystal structure of Ilmenite has ensured alternate Fe and Ti layers perpendicular to hexagonal c-axis with overriding oxygen layers. In each alternating layer Fe^{2+} ions are coupled ferromagnatically with their moments aligned parallel/antiparallel to hexagonal c-axis below its Neel breakdown.[20]

In this study, Highly-ordered hybrid ferromagnetic–Ilmenite core–shell nanostructures have been fabricated. Ferromagnetic Ni (NiFe) and $FeTiO_3$ served as core and shell of hybrid core-shell nanostructures, respectively. We have investigated the microstructural and magnetic properties of these core–shell nanostructures. The purpose of this study is to explain exchange bias mechanism from the exchange coupling between antiferromagnetic shell and ferromagnetic core. The combined FM/AFM functionalities of current study are important for future devices.

Methods

The chemical solution for $FeTiO_3$ (FTO) shell was prepared by using iron nitrate ($Fe(NO_3)_2$; Alfa Aesar>98%), titanium butoxide ($C_{16}H_{36}O_4Ti$; Energy Chemical, 98%) and ethylene glycol monobutyl ether ($C_3H_8O_2$; Sinopharm Chemical Reagent Beijing Co., Ltd., >99%). All chemicals were used without any further purification. The chemical precursors used for Ni metal and permalloy were iron

[a,*] Beijing National Laboratory for Condensed Matter Physics, Institute of Physics,Chinese Academy of Sciences, Beijing 100190, China. E-mail: usman_cssp@yahoo.com; xfhan@iphy.ac.cn.
[b] Centre for high energy physics, university of the Punjab, Lahore, Pakistan.
†Electronic Supplementary Information (ESI) available. See DOI:10.1039/x0xx00000x

nitrate ($Fe_2(SO_4)_3$; Alfa Aesar>98%), nickel sulfate ($NiSO_4 6H_2O$; Alfa Aesar>98%) and boric acid (H_3BO_3 ; Alfa Aesar>98%). Highly ordered anodized aluminum oxide (AAO) nano-membranes with average diameter of 100nm, nominal thickness of 65µm and density of ~10^9 pores/cm^2 were synthesized by ordinary two-step electrochemical process. Whereas, templates with diameter of 200nm were purchased from commercially available Whatman International Ltd.

The FTO nanotubes were prepared by sol-gel method. Sol-gel generally evolves four step synthesis route starting from solution preparation, gelation, drying and accomplish at densification. The starting solution was optimized and prepared as follows: equimolar solution (0.4M) of high purity Iron nitrate and Titanium butoxide with pH value of 0.35 was dissolved in Ethylene glycol. To maintain pH of the solution HNO_3 was added in the solution. Herein, it is also worth mentioning that HNO_3 controls extra phases of the materials. Gelation of the solution was obtained after continuous stirring for 1h at room temperature (RT). AAO templates with two different pore sizes: 200 nm and 100 nm were then dipped into the sol for 20 min. The excess solution on the surface of template was wiped off. Later, densification of the gel-coated templates was performed at 680℃ for 1h followed by drying process. To avoid cracks or breakage in templates 10℃/min heating and cooling temperature was set to attain required nanotubes in nano-channel of the AAO templates.

The next step towards core-shell structure formation was the electrochemical deposition of Ni and permalloy. 100 nm diameter has been used for core-shell nanowires whereas 200 nm has been used for core-shell nanotubes synthesis. The complete electrodeposited synthesis route is well-explained in supplementary data. The detailed synthesis process of core-shell nanostructures is illustrated in Fig. 1.

The structural analysis of the samples has been done by X-ray diffraction (XRD: RIGAKU-D/MAX-2400, Cu Kα, λ = 0.154056 nm). The morphology of nanostructures was collected by field emission scanning electron microscopy (FE-SEM: Hitachi S-4800) and transmission electron microscopy (TEM: JEOL 2011). Compositional analyses were performed with energy dispersive X-ray spectroscopy (EDS) integrated with FE-SEM. RT magnetic properties were measured by vibrating sample magnetometer (VSM: Microsense EV-9). Whereas, low temperature magnetic measurements were carried out using physical property measurement system (PPMS-model, 9T).

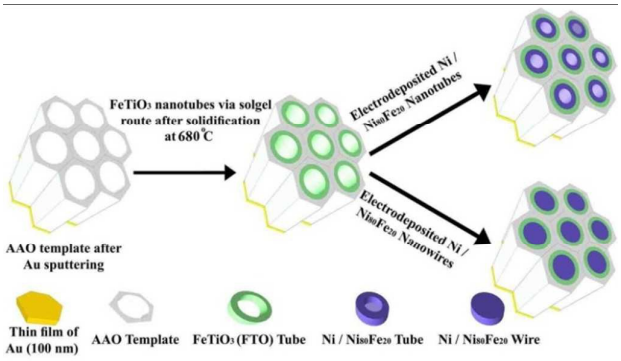

Fig. 1 Schematic for the synthesis procedure of FTO-Ni(permalloy) nanowires and nanotubes on alumina templates.

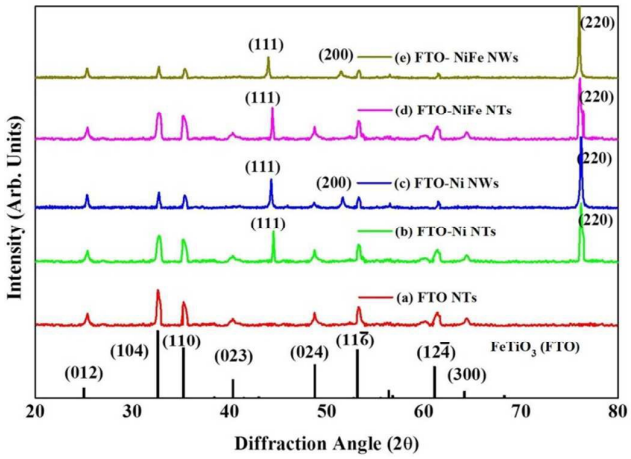

Fig. 2 (Color online) Structural analyses for (a) FTO nanotubes and below are indexed peaks following (01-075-1211) diffraction card (b) Ni-FTO nanotubes (c) Ni-FTO nanowires (d) permalloy-FTO nanotubes (e) permalloy-FTO nanowires. For (b-e) the peaks are indexed following the fcc lattice diffraction pattern.

Results and Discussion

Crystal structure information of FTO NTs determined by XRD is shown in Fig. 2a. FTO NTs demonstrated rhombohedral crystal structure with space group R$\bar{3}$. The peak positions at 2ϑ = 32.59, 35.258 and 48.73 corresponds to (104), (110) and (11$\bar{6}$) planes, respectively. It has been analyzed that XRD pattern of FTO NTs agrees well with standard pattern (JCPDS 01-075-1211) without any impurity phases. The Bragg peaks are broad which results due to relatively small crystallite size. Similar results have been reported in literature for the case of flowerlike nanostructure.[21] It is worth to mention that annealing temperature strongly affect the crystal structure of Ilmenite. Amorphous pattern without any impurity peak has been reported in temperature range of 400-700 ℃.[22]

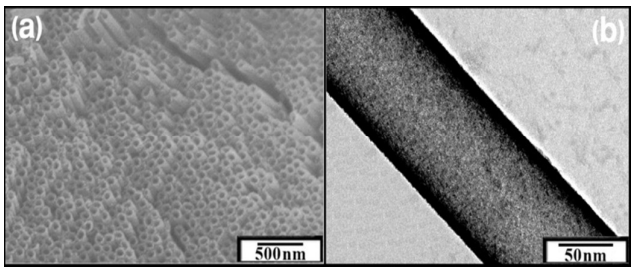

Fig. 3 Morphology of FTO nanotubes with 100 nm diaometer (a) SEM (b) TEM.

Sharp and highly crystalline Ilmenite Bragg's peaks were found as temperature increases from 400 to 700 ℃ with no change in phase composition.[21-22] SEM and TEM images of FTO NTs have been shown in Fig. 3(a) and 3(b), respectively. FTO NTs were synthesized within 100 nm (for core-shell NWs) and 200 nm (for core-shell NTs) diameter of nano-membranes. Densification of FTO NTs was occurred at 680 ℃ because of two appropriate reasons (1) crystal structure maintain phase composition without any impurity phases (2) diffusion between membranes and electrodeposited core-structure starts which effects on magnetic properties at higher temperature. Afterwards, Ni/permalloy NWs and NTs were electrodeposited within FTO sol-gel coated nano-channels for the investigation of magnetic properties. Fig. 2(a-c) depicts XRD patterns of Ni/permalloy NWs and NTs embedded in FTO nano-channels. Bragg's planes (111), (200) and (220) at 2ϑ = 44.3, 51.5 and 78.3 corresponds to fcc structure of Ni NTs and NWs as shown in Fig. 2(a) and 2(b), respectively. In addition, due to the increase of Fe contents, for permalloy composition, there is a slight shift in Ni diffraction peaks towards low angle which is attributed to lattice expansion (Fig. S1). The behavior for Iron doping in permalloys similar with $Ni_{1-x}Fe_x$ (x=0-1) thin films[23] and permalloy NWs.[24, 25] where, growth of lattice parameters with Fe contents has been observed. However, small shift in lattice parameter in our case might be attributed to the larger ionic radius of Nickel than iron. The morphology of core-shell NWs and NTs characterized by SEM and TEM with different magnifications has been presented in Fig. 4 and Fig. 5.

The length and diameter of NTs were consistent with AAO membranes. Thickness of NTs for the case of core-shell nanostructure has strong effect on magnetic properties.[10] In present case, shell with average thickness of ~25 nm was achieved which is good enough for magnetic response as shown in Fig. 3b. Compositional analysis has confirmed that Iron and Titanium are in 1:1 ratio which is in good agreement with XRD as shown in Fig. S2.

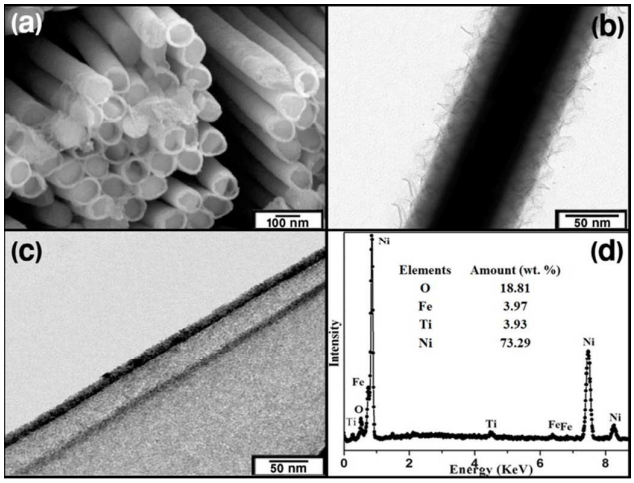

Fig. 4 (a) SEM micrograph for FTO-Ni core-shell nanowires (b) TEM image of single Ni-FTO core-shell nanowire with FTO wall thickness of 25nm (c) Ni-FTO core-shell nanotubes and (d) compositional analysis obtained from EDS.

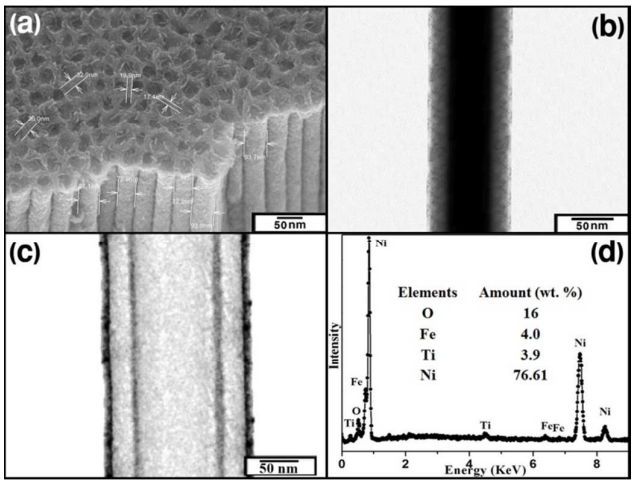

Fig. 5 (a) SEM micrograph for permalloy-FTO core-shell nanowires (b) TEM image of single permalloy-FTO core-shell nanowire with FTO wall thickness of 25nm (c) permalloy-FTO core-shell nanotubes, and (d) compositional analysis obtained from EDS.

Fig. 4 and 5 illustrates SEM and TEM images of Ni/permalloy deposited FTO cores-shell NWs and NTs. It can be seen that morphology of nanostructures is clean and homogeneous as shown in Fig. 4a and 5a. The growth of NWs was uniform with good density as shown in Fig. S3. Pore diameter of 100 nm and 200 nm was used for the synthesis of NWs and NTs, respectively. In case of FTO-Ni(permalloy) core-shell NWs the average wall-thickness of FTO tubes is ~25 nm which is in contrast with diameter of core structure as shown in Fig. 4b and Fig 5b. This was the reason for the selection of AAO nano-membranes with 200 nm diameter for the synthesis of FTO-Ni(permalloy) core-shell NTs. EDS gives the information of electrodeposited Ni in FTO tube as shown in Fig. 4d. There is slight difference of Iron and Titanium contents in compositional analysis of FTO-permalloy NWs and NTs which defines iron doping for the formation of permalloy (Fig. 5d). Therefore, EDS is another tool which supports XRD results about permalloy NWs and NTs. It is necessary to mention that to get highly oriented, fine and smooth morphology of NWs and NTs, etching solution with appropriate molar ratio, etching environment and sample cleaning is very important. The detailed process for sample preparation has been explained in supplementary data.

Multiferroic materials have attracted interest due to their potential applications in sensors and storage devices because of their instantaneous ferroelectric and ferromagnetic properties. Until now, there are few materials which have been reported because of their multiferroic response. Varga *et al.* have reported about multi-ferroic nature of FTO at and below room temperature.[26] In present work, we have measured ferroelectric properties of FTO embedded in AAO membrane. The P-E loop indicates that there is small spontaneous polarization with remnant polarization of 12.5 μCcm^{-2} and coercive field of 40$kVcm^{-1}$. The presence of spontaneous polarization depicts that FTO must be ferroelectric at room temperature (Fig. 6).

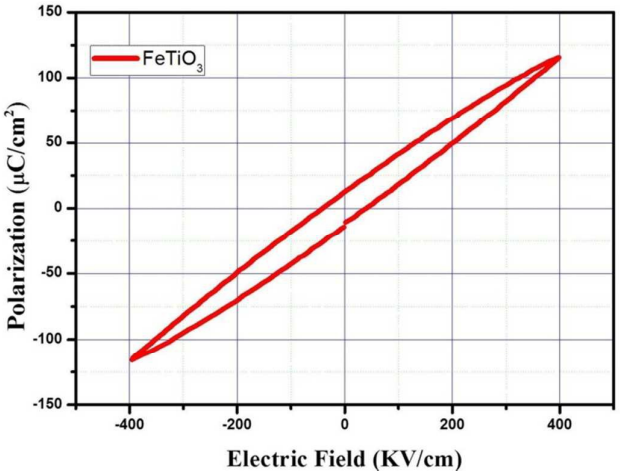

Fig. 6: P-E loop of FTO nanotubes at room temperature

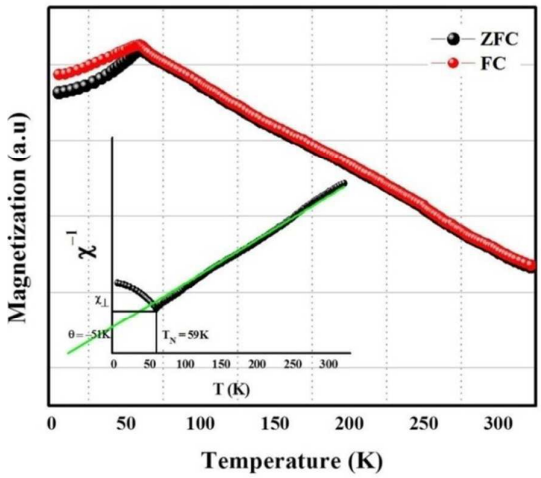

Fig. 7 Temperature dependent magnetization of FTO Shell under the field of 100 Oe. Inset of figure depicts a graph between magnetic susceptibility across temperature with Neel temperature of 59K

Antiferromagnetic response of FTO has been reported at Neel temperature of ~59K.[15-16] Temperature dependent magnetization has been shown in Fig. 7, where zero field cooling (ZFC) and field cooling (FC) effect was measured under the field of 100Oe. It can be seen that magnetic moments of both ZFC and FC curve were enhanced with decrease in temperature. A sharp peak occurred at a temperature of 59K where bifurcation between FC and ZFC occurred. Below Neel temperature magnetic moments of both FC and ZFC curve were decreased. A plot between inverse of magnetic susceptibility and temperature has been shown in the inset of Fig. 6 where data was compatible with Curie-Weiss law with equation:

$$1/\chi = \frac{T-\theta}{C}$$

where, χ is magnetic susceptibility, θ and C are Currie-Weiss temperature and constant respectively.

Fitting result is marked with green line with $\theta = -51$K and C = 3.102. The antiferromagnetic nature of FTO is indicated by negative value of θ.

The experimental value of magnetic moment is generated with

$$\mu_{exp}^2 = \frac{3k_B C}{N_A \mu_B^2}$$

Where, k_B is Boltzmann's constant (1.38 x 10^{-16} erg/K), N_A is Avogadro's number (6.02 x 10^{23} mole^{-1}) and μ_B is Bohr magnetron (9.27 x 10^{-21} erg/Oe). The estimated value of μ_{exp} was 4.979 μ_B which is slightly higher than theoretical magnetic moment of FTO (4.899 μ_B). This is evidence that only FTO without any impurity phases is deposited in AAO membrane which supports the XRD results.

Magnetic hysteresis loops measured for Ni and permalloy deposited FTO core-shell NWs and NTs at room temperature and 5K are shown in Fig. 8. For FTO-Ni(permalloy) NWs, magnetic moment at saturation field is 4.2 m.emu and 16.7 m.emu respectively and magnetic coercivity is Hc(∥)=581Oe, Hc(⊥)=79Oe (Ni-FTO NWs) and Hc(∥)=795Oe, Hc(⊥)=360Oe ($Ni_{80}Fe_{20}$-FTO NWs) as shown in table 1 and Fig. 8(a,c). The addition of iron contents in core leads to enhance overall magnetic properties of Ni-FTO core-shell structure. The similar magnetic response is observed for Ni-FTO as well as for permalloy-FTO NTs. On the other hand, saturation magnetic moment and coercivity decreases for the cases of core-shell NTs compared with that of core-shell NWs.

Furthermore, in case of core-shell NTs, easy direction of magnetization orients perpendicular to tubes long axis as shown in Fig. 8(b,d). There are several reports in literature which demonstrated perpendicular easy direction of magnetization for magnetic nanotubes.[27-28] Easy direction of magnetization in FTO-Ni(permalloy) core-shell NWs is along wire axis as a result of strong magnetic shape anisotropy but strong magnetostatic interactions

Table 1. Experimental values of magnetic parameters of core-shell nanostructure.

		FTO-Ni		FTO-$Ni_{80}Fe_{20}$	
		NWs	NTs	NWs	NTs
Coercivity (Oe)	H_c (∥)	581	125	795	90
	H_c (⊥)	79	169	360	174
Saturation Field (Oe)	H_s (∥)	4515	5989	3969	5994
	H_s (⊥)	7975	4986	9016	4207
Anisotropic Field (Oe)	H_a	6161	500	6978	666
Anisotropic Constant	K	12322	~152	~58266	~266

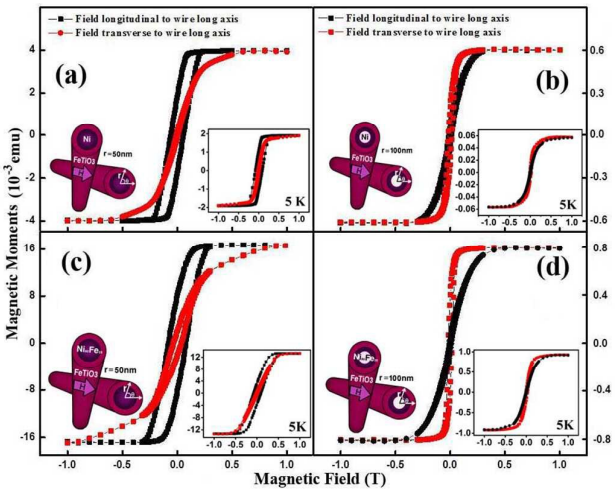

Fig. 8 Room temperature hysteresis loops of (a) Ni-FTO core-shell nanowires (b) Ni-FTO core-shell nanotubes (c) permalloy-FTO core-shell nanowires (d) permalloy-FTO nanotubes for magnetic field applied longitudinal and transverse to wire long axis, whereas insets represent their corresponding hysteresis loops at 5K.

induce easy axis perpendicular to nanotube axis. Magnetocrystalline anisotropy is meaningless because of polycrystalline nature of electrodeposited nanostructures.

Magnetic anisotropy with coercivity H_c makes magnetic system interesting for applications in microwave filters and high density data storage.[29] Magnetic anisotropic field for core-shell NWs and NTs can be calculated with hysteresis loops determining the area between perpendicular and parallel M-H loop by using, $H_a = \int[M_\perp(H) - M_\parallel(H)/M_s]dH$, where $M_\perp(H)$ and $M_\parallel(H)$ are the magnetization when field was applied perpendicular and parallel to nanowire long axis, M_s is ordinary used saturation magnetization quantity. Similar approach has been adopted by Nasirpouri *et al.* to find magnetic anisotropy for CoP nanowires.[30] Magnetic anisotropic constant can thus be estimated with $K = M_s H_a/2$. Calculations determined that magnetic anisotropic constant is greater for the case of permalloy nanowires than other geometries defined here. The numerical values of K are tabulated in table 1. This can be attributes to greater value of saturation magnetization. The estimated magnetic properties are mentioned in table 1. We suggested that permalloy-FTO core-shell nanostructures might represent optimal magnetic properties for industrial applications, for example, automotive systems and wireless communications where broader bandwidths and smaller sizes are required.[31]. Magnetic nanowire substrates made of embedded nanowires in AAO templates are most suitable candidates for such applications because of their applicable magnetic properties and opportunity to construct tuneable nanomagnetic devices.[32]

In case of core-shell nanostructures exchange bias (EB) is another interesting mechanism which gives information about exchange interactions at FM/AFM interface. This phenomenon has been investigated in several magnetic systems, for example, FM/AFM layer in thin films and shell coated nanoparticles.[33] Mostly, thin films have been focused to study the EB due to good control of thickness and textures.[34-36] There are a few studies which have been reported to explain this mechanism in 1D nanostructures. Theory of EB is still in developing phase but it is strong believe that there are several parameters which can affect it, such as thickness of AFM, interface roughness, spin configuration, and grain sizes.

The EB systems are characterized by their Neel temperature (T_N) which is responsible for the ordering of magnetic moments in antiferromagnetic materials. There are three further possibilities depending on anisotropy of antiferromagnetic material. If magnetic anisotropy of AFM material is large then EB mechanism occurs at AFM/FM interface while in other case only coercivity H_c of the system increases. Both effects are also observed simultaneously as a result of AFM anisotropy. It has been reported that strong anisotropy is present in FTO due to uncompensated spins of iron contents. [37, 38] In this report, we have investigated EB properties of ferromagnetic Ni/permalloy NWs and NTs embedded in AFM FTO for the first time. Field cool (FC) and zero field cool (ZFC) magnetic hysteresis loops were measured at 5K after field cool under 1T external magnetic field, are shown in Fig. S4. ZFC hysteresis loops for all samples showed symmetrical behavior, whereas FC loops are

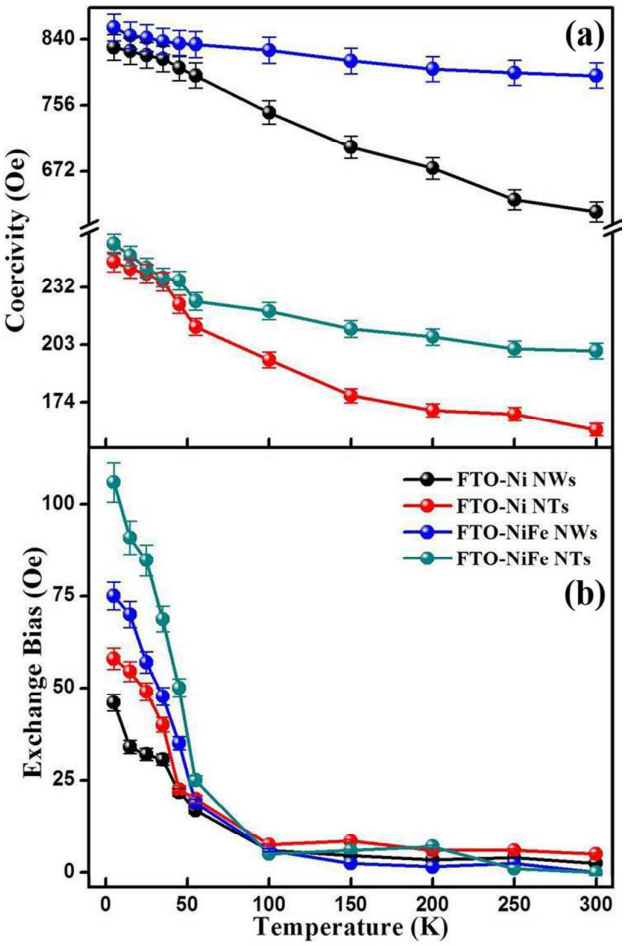

Fig. 9 Temperature dependence of (a) coercivity, and (b) exchange bias after field cool under magnetic field of 1T.

shifted in opposite direction to cooling field. This is because, during zero field cool, the spins of magnetic moments in AFM remain dis-orient while in field cool process; all the magnetic moments become parallel to the applied magnetic field.

Another remarkable difference occurs in Fig. S4(c) where magnetization is clearly larger in FC loop. It is believed that exchange bias field generally originates through interfacial coupling between ferromagnetic Ni/permalloy core and antiferromagnetic FTO shell. Whereas, difference in magnetic properties at 1T field cool and zero field is probably because of aligned uncompensated spins after field cool in AFM FTO shell. Temperature dependent exchange bias and magnetic coercivity of these systems is depicted in Fig. 9. EB is observed in all samples and it appeared below Neel temperature (T_N = 59K). Below this temperature there are free magnetic moments because of iron presence in FTO which we have discussed earlier in detail and play vital role for the mechanism under study. Coercivity H_c decreased monotonically from low temperature to room temperature whereas exchange bias EB is maximum at low temperature and vanished at or above Neel temperature of AFM FTO. There are several studies where scientists have demonstrated increasing trend of both H_c and *EB* below Neel temperature.[34,37] However, coercivity of elongated systems arises due to strong effect of magnetic anisotropy. So, we argue that coercivity of FTO-Ni(permalloy) increases depending on magnetic anisotropy. Furthermore, the results showed that temperature dependent coercivity unambiguously causes exchange bias mechanism and due to decrease in coercivity, exchange bias also decreases by increasing temperature 5K to 59K. The trend is similar for FTO-Ni(permalloy) core-shell nanostructures. Another possible justification to this enhancement might be endorsed to the presence of uncompensated spins at FTO (AFM) and Ni/permalloy (FM) interface.

Conclusions

In summary, we have presented a new hybrid core-shell nanostructure consisting of $FeTiO_3$ antiferromagnetic shell and Ni/permalloy ferromagnetic core. Firstly, growth of $FeTiO_3$ nanotubes in alumina templates with average wall thickness of 25nm was controlled via sol-gel method. Afterwards, Ni/permalloy nanowires and nanotubes were electrodeposited in FTO nano-channels. Microstructural characterizations confirmed Ilmenite phase of FTO and peak shift towards lower angle has been observed due to the doping of iron contents in Ni core. SEM and TEM micrographs depicted clean, smooth and homogeneous growth of core-shell nanostructures. Low temperature magnetic characterizations predicted that FTO aligned its magnetic moments at 59K. The estimated value of magnetic moments was 4.979 μ_B which is slightly higher than theoretical magnetic moment of FTO (4.899 μ_B). This is the evidence that only FTO without any impurity phases is deposited in AAO membrane which supports XRD results. Exchange anisotropy has been observed due to the enhancement in magnetic coercivity after field cool under applied magnetic field of 1T. Magnitude of exchange bias can be controlled by external magnetic field at low temperatures. The exchange bias phenomenon has been observed below Neel temperature due to perfect alignment of magnetic moments in AFM. This shows that once the ordering of magnetic moments in AFM shell is lost then exchange bias vanishes, indicating vital role performed by AFM shell in the observed exchange bias interaction. Therefore, we suggested that FTO-permalloy core-shell nanostructure might represent optimal magnetic properties for industrial applications, for example, automotive systems and wireless communications where broader bandwidths and smaller sizes are required. Magnetic nanowired substrates made of embedded nanowires in AAO templates are most suitable candidates for such applications because of their applicable magnetic properties and opportunity to construct tunable nanomagnetic devices.

Acknowledgements

The project was supported by the State Key Project of Fundamental Research of Ministry of Science and Technology [MOST, No. 2010CB934401], National Natural Science Foundation of China [NSFC, Grant No. 11374351 and 11434014].

References

1 F. J. Heiligtag and M. Niederberger, *Materials Today*, 2013, **16**, 262.
2 Z. Sun, T. Liao, Y. Dou, S. M. Hwang, M. S. Park, L. Jiang, J. H. Kim and S. X. Dou, *Nature Communications*, 2014, **5**, 3813.
3 A. I. Gapin, X. R. Ye, J. F. Aubuchon, L. H. Chen, Y. J. Tang and S. Jin, *Journal of Applied Physics*, 2006, **99**, 08G902.
4 4S. S. P. Parkin, M. Hayashi and L. Thomas, *Science*, 2008, **320**, 190.
5 L. T. Patrick D. McGary, JiaZou, Bethanie J. H. Stadler, Patrick R. Downey, and Alison B. Flatau, *Journal of Applied Physics*, 2006, **99**, 08B310.
6 F. L. B. Ye, D. Cimpoesu, J.B. Wiley, J.-S. Jung, A. Stancu, L. Spinu, *Journal of Magnetism and Magnetic Materials*, 2007, **316**, e56.
7 T. Seto, H. Akinaga, F. Takano, K. Koga, T. Orii and M. Hirasawa, *Journal of Physical Chemistry B*, 2005, **109**, 13403.
8 J. Sort, V. Langlais, S. Doppiu, B. Dieny, S. Surinach, J. S. Munoz, M. D. Baro, C. Laurent and J. Nogues, *Nanotechnology*, 2004, **15**, S211.
9 T. Maurer, F. Zighem, F. Ott, G. Chaboussant and G. André, *Physical review B*, 2009, **80**, 064427.
10 D. W. Shi, J. Chen, S. Riaz, W. Zhou and X. Han, *Nanotechnology*, 2012, **23**, 305601.
11 J. B. Yi, J. Ding, B. H. Liu, Z. L. Dong, T. White and Y. Liu, *Journal of Magnetism and Magnetic Materials*, 2005, **285**, 224.
12 A. Kohn, A. Kova, R. Fan, G. J. McIntyre, R. C. C. Ward and J. P. Goff, *Scientific Reports*, 2013, **3**, 2412.
13 J. S. Moodera and J. Nassar, Annual Review of Materials Science, 1999, **29**, 381.
14 R. L. Stamps, *Journal of Physics D: Applied Physics*, 2000, **33**, R247.
15 R. Pentcheva and H. S. Nabi, *Physical Review B*, 2008, **77**, 172405.
16 P. F. McDonald, A. Parasiris, R. K. Pandey, B. L. Gries and W. P. Kirk, *Journal of Applied Physics*, 1991, **69**, 1104.
17 T. Fujii, M. Kayano, Y. Takada, M. Nakanishi and J. Takada, *Solid State Ionics*, 2004, **172**, 289.
18 X. Tang and K. Hu, *Journal of Materials Science*, 2006, **41**, 8025.

19 F. Ye and A. Ohmori, *Surface and Coatings Technology*, 2002, **160**, 62.
20 Y. Yamaguchi, H. Kato and H. Takei, *Solid State Communications*, 1986, **59**, 865.
21 T. Tao, A. M. Glushenkov, H. Liu, Z. Liu, X. J. Dai, H. Chen and a. Y. C. Simon P. Ringer, *Journal of Physical Chemistry C*, 2011, **115**, 17297.
22 J. Ru, Y. Hua, C. Xu, J. Li, Y. Li, D. Wang, K. Gong, R. Wang and Z. Zhou, *Ceramics International*, 2014, **40**, 6799.
23 M. S. Salem, P. Sergelius, R. Zierold, J. M. M. Moreno, D. Gorlitz and K. Nielsch, *Journal of Materials Chemistry*, 2012, **22**, 8549.
24 B. Glaubitz, S. Buschhorn, F. Brussing, R. Abrudan and H. Zabel, *Journal of Physics-Condensed Matter*, 2011, **23**, 254210.
25 N. Adeela, K. Maaz, U. Khan, S. Karim, M. Ahmad, M. Iqbala, S. Riaz, X. F. Han and M. Maqbool, *Ceramics International*, 2015.
26 T. Varga, A. Kumar, E. Vlahos, S. Denev, M. Park, S. Hong, T. Sanehira, Y. Wang, C. J. Fennie, S. K. Streiffer, X. Ke, P. Schiffer, V. Gopalan and J. F. Mitchel, *Physical Review Letters*, 2009, **103**, 047601.
27 X. F. Han, S. Shamaila, R. Sharif, Jun-Yang Chen and a. D.-P. L. Hai-Rui Liu, *Advanced Materials*, 2009, **21**, 4619.
28 J. Y. Chen, N. Ahmad, D. W. Shi, W. P. Zhou and X. F. Han, *Journal of Applied Physics*, 2011, **110**, 073912
29 M. Darquesa, J. Spiegelb, J. D. T. Medinaa, I. Huynenb and L.Pirauxa, *Journal of Magnetism and Magnetic Materials*, 2009, **321**, 2055.
30 F. Nasirpouri, S. M. Peighambari, A. S. Samardak, A. V. Ognev, E. V. Sukovatitsina, E. B. Modin, L. A. Chebotkevich, S. V. Komogortsev and S. J. Bending, *Journal of Applied Physics*, 2015, **117**, 17E715.
31 J. Spiegel and I. Huynen, Solid State Phenomena, 2009, **152**, 389.
32 C. E. C. Gonzalez, J. D. L. T. Medina, L. Piraux and A. Encinas, *Nano Letters*, 2011, **11**, 2023.
33 B. Kuerbanjiang, U. Wiedwald, F. Haering, J. Biskupek, U. Kaiser, P. Ziemann and U. Herr, *Nanotechnology*, 2013, **24**, 455702.
34 A. E. Berkowitz and K. Takano, *Journal of Magnetism and Magnetic Materials*, 1999, **200**, 552.
35 J. Nogues and I. K. Schuller, *Journal of Magnetism and Magnetic Materials*, 1999, **192**, 203.
36 H. Zabel and S. D. Bader, *Berlin Heidelberg*, 2008, **227**.
37 H. Hojo, K. Fujita, H. Ikeno, T. Matoba, T. Mizoguchi, I. Tanaka, T. Nakamura, Y. Takeda, T. Okane and K. Tanaka, *Applied Physics Letters*, 2014, **104**, 112408.